Int. J. Electrochem. Sci., 12 **(2017)** 1863 – 1873, doi: 10.20964/2017.03.59

International Journal of
ELECTROCHEMICAL
SCIENCE
www.electrochemsci.org

Short Communication

Electrodeposition of Co-B hard coatings: characterization and tribological properties

A. Martínez-Hernández[1], *Y. Meas*[1], *J.J. Pérez-Bueno*[1], *L.A. Ortíz-Frade*[1], *J.C. Flores-Segura*[1], *Alia Méndez-Albores*[2], *G. Trejo*[1,*]

[1] Laboratory of Composite Materials and Functional Coatings. Center for Research and Technological Development in Electrochemistry (CIDETEQ). Parque Tecnológico Sanfandila, Pedro Escobedo, A.P. 064, C.P. 76703, Querétaro, México.
[2] Center of Chemistry-ICUAP Benemérita Universidad Autónoma de Puebla, Ciudad Universitaria Puebla, 72530 Puebla, México
[*]E-mail: gtrejo@cideteq.mx

Received: 8 December 2016 / *Accepted:* 19 January 2017 / *Published:* 12 February 2017

Electrodeposited Co-B alloy coatings were formed using dimethylamine borane (DMAB) as the boron source. The results showed that the concentration of boron in the coatings increased with increasing concentration of DMAB in the electrolytic bath. Additionally, Co-B bond formation and the presence of DMAB in the coatings were proposed on the basis of the results obtained by glow discharge spectrometry and X-ray photoelectron spectroscopy. The influence of boron concentration in the coating on the tribological characteristics of hardness, friction coefficient and wear volume are discussed. Co-B coatings without microfissures on their surface were obtained when the concentration of boron in the coating was between 2.9 and 3.0 wt.%. Co-B coatings with these boron concentrations exhibited a hardness value of 818 HV, which is higher than Ni-B coatings but lower than hard chromium coatings (867 HV). The volume of wear and friction coefficients of the Co-B coatings with 2.9 and 3.0 wt.% were also lower than those reported for Ni-B coatings.

Keywords: Co-B Alloy Coatings; Electrodeposition; Hardness; Hard Coatings; Wear Volume.

1. INTRODUCTION

For many decades, hard coatings have been widely used in the aerospace and automotive industries to protect tools against corrosion and wear. Because of their high wear resistance, low coefficient of friction (<0.3) and intrinsic high hardness (600-1000 HV), hard chromium films are among the most broadly used functional coatings. Although hard chromium coatings contain mostly

trivalent chromium, which is considered safe, most hard chromium processing techniques involve a high vapour pressure of mist containing hexavalent chromium derived from chromic acid, which is highly toxic and a known carcinogen. Because of the toxicity of chromium compounds, maximum exposure levels of chromate ions are regulated. The US Department of Labor´s Occupational Safety and Health Administration (OSHA) has reduced the permissible exposure limit for hexavalent chromium from 52 $\mu g/m^3$ to 5 $\mu g/m^3$ of air for 8-hour time-weighted averages. In addition to tighter limits on air exposure limits, the Environmental Protection Agency (EPA) has also set new limits for chromium in water, recognizing that the electrodeposition of chromium is a hazardous process. Thus, a great need clearly exists to replace electroplated chromium coatings with alternative coatings that match or exceed the physical properties of chromium coatings and are biocompatible and safe.

In recent years, electroless and electrodeposited Ni-B [1-8] and Ni-P [9,10] alloys with nanocrystalline and amorphous structures have been considered as potential replacements for hard chromium. Several studies have shown that Ni-P and Ni-B coatings are amorphous in their plated condition and before heat treatment to 350 °C, where the phases nickel phosphide (Ni_3P) [11,12] and nickel boride (Ni_3B) [13,14] are produced in the respective coatings. Depending on the concentration of the new phase of N_3P and Ni_3B, the hardness of the coatings increased substantially from 850 to 1300 HV after the heat treatment [6,15,16]. Despite the nickel compounds providing good performance and durability, nickel is also listed by the EPA as a priority pollutant; it is considered one of the 14 most toxic heavy metals. Thus, coatings containing nickel are, at best, a short-term solution.

Cobalt has been reported to have a hardness similar to that of nickel; it tends to yield boron alloys Co_3B, Co_2B and CoB after thermal treatment at temperatures ranging from 300 to 500 °C [17,18]. Additionally, cobalt is not considered a heavy metal that negatively affects human health [19]. Therefore, cobalt may be a viable option for coatings that can replace hard Cr due to its similar or improved mechanical properties.

Cobalt-boride (Co-B) alloys can be prepared using several methods; *e.g.*, Li *et al.* [20] produced an amorphous Co-B alloy by simple chemical reduction from their respective salts. Similarly, using chemical reduction of cobalt ions in an aqueous medium, Hui *et al.* [21] prepared Co-B nanochains with borohydride as the reducing agent. Lu *et al.* [22] used an applied magnetic field in the synthesis of Co-B alloy nanowires via reduction of $CoCl_2$ with $NaBH_4$ in solution. Additionally, Yi *et al.* [23] prepared various Co_x-B (x = 1, 2, 3) compounds using an arc melting method. All of the aforementioned alloys exhibited good electrochemical reaction reversibility and could be used as high-capacity electrodes. Because of their high discharge capacity in alkaline solutions, the Co-B alloys have attracted attention for use as high-energy-density anodes [24-27], as materials for hydrogen storage [28] and as catalysts for hydrogen production via hydrolysis of boron-hydrides [29]. Despite the aforementioned technological applications of Co-B alloys, the literature contains only a few studies on their electrodeposition, with no description of their tribological properties or their use as potential hard coatings. Subramanian *et al.* [30] reported an increase in the amount of boron in amorphous Co-B alloys when the current density was increased using an alkaline medium in the presence of citrate. Bekish *et al.* [31] produced a Co-B alloy by electrodeposition with the decahydro-*closo*-decaborate anion as the boron source, suggesting a chemical interaction between boron and cobalt atoms.

The aim of this work was to study the electrodeposition of Co-B alloys and the effect of boron content on their physical properties, including their hardness, resistance to wear and friction coefficients.

2. MATERIAL AND METHODS

Co-B alloy coatings were electrodeposited from a base solution, S_0, of composition: 0.14 M $CoCl_2 \cdot 6H_2O$ + 0.32 M H_3BO_3 + 2.8 M KCl at pH = 5.0 ± 0.3; dimethylamine borane (DMAB) was used at concentrations of 0, 1, 3, 5, 7 and 10 g L^{-1} as a source of boron. These solutions were prepared immediately prior to each experiment using deionized water (18 MΩ cm) and analytical-grade reagents of the highest purity available (J.T. Baker). A methacrylate parallel-plate cell with an interelectrode distance of 5 cm was used for the formation of the Co-B coatings, and the temperature of the electrolytic bath was maintained at 25 °C. A graphite plate was used as the anode, and plates of AISI 1018 steel with an exposed area of 2.5 × 5.5 cm^2 were used as the cathode. Before each experiment, the cathode was cleaned with degreasing solution. The electrodeposition current density (0.011 A cm^{-2} over 20 min) was selected on the basis of additional testing (results not presented here) using a Hull cell. The coating thickness was approximately 10 μm.

The electronic structure of the surfaces and the chemical states of the coatings were analysed by X-ray photoelectron spectroscopy (XPS) (Thermo Scientific, model K-Alpha). The elemental composition of the coatings as a function of the thickness was obtained by glow discharge spectrometry (GDS) (Horiba, model GD Profiler 2). The morphology of each coating was evaluated using scanning electron microscopy (SEM) (JEOL, model JSM-6510LV) in conjunction with energy-dispersive X-ray spectroscopy (EDS) (Bruker, model Quantax 200). Atomic force microscopy (AFM) (Asylum Research, model MFP-3D) was used in tapping mode to observe the deposited Co-B alloys on the steel substrates. These measurements were performed in air (*ex situ*) using silicon nitride AFM tips. All images were obtained at 1.5 Hz; they are presented in the so-called height mode, where the highest portions appear brighter.

A Matsuzawa MXT-ALFA Vickers microhardness tester with a 10 g load applied for 15 s was used for hardness measurements. The final value reported for the coating hardness was the average of ten measurements.

Wear tests were performed on a reciprocating ball-on-disk tribometer (CSM tribometer) in air at a temperature of approximately 25 °C and a relative humidity of approximately 39% under dry, non-lubricated conditions. Balls (3-mm diameter) made of WC with a hardness of 3500 HV were used as the counter body in the wear tests. All wear tests were performed under a 2 N load at a sliding speed of 4.2 cm s^{-1}. The friction coefficient and sliding time were automatically recorded during the tests. The wear volume was measured according to the ASTM G99 standard method [32]. Three wear tests were conducted for each sample.

3. RESULTS AND DISCUSSION

3.1 Electrodeposition and characterization of the chemical composition and surface electronic structure of the Co-B coatings

Co-B alloy coatings were electrodeposited under galvanostatic conditions at 0.011 mA cm^{-2} for 20 min from solution base S_0 at various DMAB concentrations ranging from 0 to 10 g L^{-1}. The elemental composition profiles for the Co-B coatings were determined by GDS. Fig. 1 shows the typical elemental composition profile of a Co-B coating. The sample analysis was conducted at successive depths until the substrate (Fe) was reached. The thickness of the Co-B coatings was approximately 10 ± 0.3 µm. At the surface of the coatings (erosion time < 5 s), a higher concentration of oxygen was present, associated with surface oxidation. After the oxide layer was removed from the surface, the oxygen concentration decreased, and the Co, N, B and C signals were observed. During the analysis, the relative concentration of Co was constant at ~97 wt.%; this concentration decreased after 50 s of erosion because of the onset of the substrate (Fe) signal, which indicated that the substrate/coating interface (Fe/Co-B) was reached. Additionally, the boron in the alloy behaved similarly to Co in the same time range, although at lower concentrations (~3 wt.% B), suggesting that Co and B co-deposit. In this regard, Brenner [33] proposed that for an aqueous electrolyte solution, the electrodeposition of boron onto the cathode surface was possible only when the boron was alloyed with another stable metal such as cobalt (induced co-deposition). Additionally, across the entire evaluated deep range, the signals of C and N were present identically to B but at different concentrations. Similarly, the signals of C and N were observed within the substrate because both were present in AISI 1018. Notably, hydrogen was not detected during the analysis, probably because its concentration in the coating was below the detection limits of the glow discharge spectrometer.

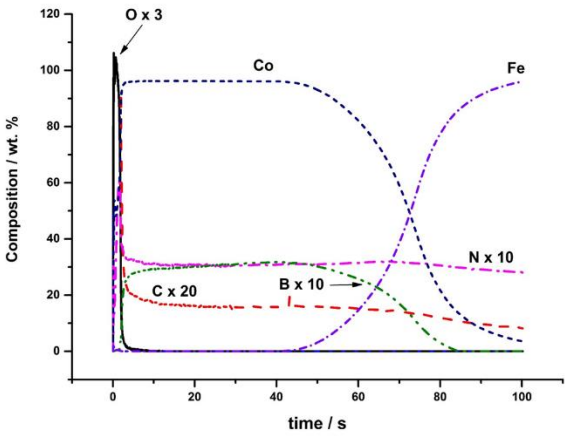

Figure 1. GDS analysis of the elemental-distribution profiles of the Co-B coatings electrodeposited under galvanostatic conditions (j = 0.011 mA cm^{-2}, t = 20 min).

Fig. 2 shows the amounts of B, N and C in the coatings (as measured by GDS) formed from electrolytic baths with different concentrations of DMAB. In the range of concentrations studied, the amounts of B, C and N in the Co-B coating exhibited a proportional relationship with the concentration

of DMAB. When the concentration of DMAB in the electrolytic bath was increased from 1 to 7 g L^{-1}, the content of B in the coating increased from 1 to 2.94 wt.%. In the case of higher DMAB concentrations, the B content in the coating reached a constant value of approximately 3 wt.%; similar concentrations have been reported by other authors [6,8] for Ni-B electrodeposited using DMAB as the boron source.

When the DMAB concentration was increased from 1 to 7 g L^{-1} in the electrolytic bath, the amount of N also increased from 1.3 to 3.5 wt.%. In the case of DMAB concentrations greater than 7 g L^{-1}, a decrease in wt.% N was observed. Notably, the B and N were present in a ratio of approximately 1, suggesting the presence of DMAB in the coating.

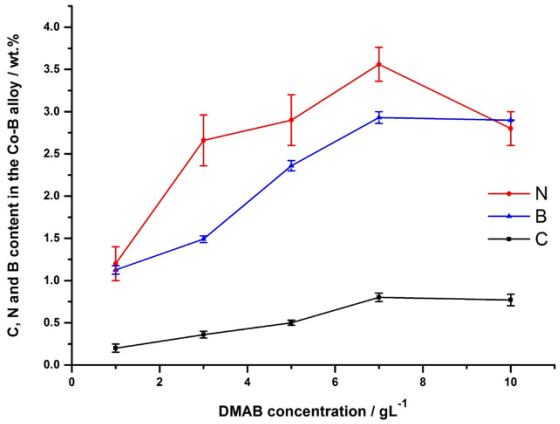

Figure 2. C, N and B contents of the Co-B alloy (wt.%) as a function of the DMAB concentration in solution.

To study the electronic interactions between the atoms in the coating, we collected XPS spectra of the Co-B coatings. Figure 3 shows typical XPS spectra obtained for the Co-B coatings; the spectra show signals for cobalt species in different oxidation states. A peak at a binding energy of 778.0 eV, which corresponds to the Co^0 state [34] is observed (Fig. 3a). A 0.2 eV decrease in the binding energy in the Co-B alloy compared with that in the pure Co standard (778.2 eV) indicates an increase in electron density around cobalt. Typical signals ranging from 780 to 790 eV demonstrate the presence of cobalt oxides (CoO, Co_3O_4) [35]. The B^0 signal was observed at 187.8 eV, which is slightly higher (0.6 eV) than that for the pure B standard (187.2 eV) (Fig. 3b). Similar results have been reported by Lee *et al.* [36] for crystallized Ni-B, suggesting that the binding energies changed because of the electron-deficient state of the boron atoms, which are intermediate between elementary boron and borides. Similarly, the signal observed at 191.48 eV corresponds to the B-N interactions of the DMAB molecules.

Other XPS signals for chemical bonds including N-B, N-C (Fig. 3c) and C-C, C-H were also observed from 392 to 404 eV and from 280 to 290 eV, respectively (Fig. 3d). Thus, the results obtained by both techniques, GDS and XPS, suggested the molecular occlusion of DMAB during the growth process of the film.

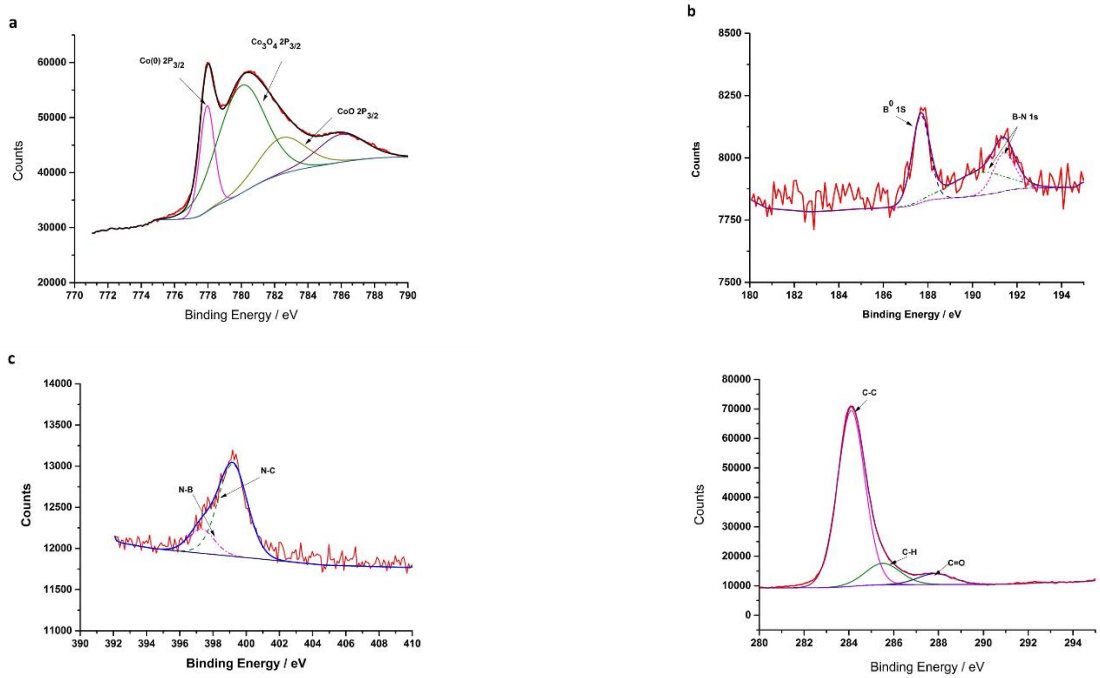

Figure 3. XPS spectra of the Co-B coatings obtained under galvanostatic conditions (j = 0.011 mA cm^{-2}, t = 20 min): a) Co $P_{3/2}$, b) B 1S, c) N 1S, and d) C 1S.

The mechanism by which boron is incorporated into Co-B coatings prepared by the electrodeposition technique has not been reported. Our GDS and XPS results suggest that DMAB molecules are adsorbed during the electrodeposition process. The binding energy of Co^0 in Co-B coatings was slightly lower than that of the pure Co^0 standard, which implies that Co is electron rich. Conversely, the binding energy of B in the coating was slightly higher than that of the pure B standard, which implies an electron-deficient element. Therefore, we propose a partial electron transfer mechanism between the electron rich (Co) and the electron deficient (B) elements in the Co-B alloy.

3.2 Morphological characterization

We analysed the surface morphology of the Co-B alloys by SEM and AFM. Fig. 4 shows SEM and AFM images of the Co-B coatings obtained from solutions S_0 containing different concentrations of DMAB (*i.e.*, coatings with different wt.% B). In the absence of DMAB (Fig. 4a) (0 wt.% B in the coating), the surface of the Co coating showed superficial micro-fissures due to the inner coating stress. Additionally, the coatings were compact, smooth, adherent and shiny. Because of these characteristics, we further characterized the coating morphology using AFM. The AFM image (see inset of Fig. 4a) shows the morphology of an amorphous Co coating.

The presence of B in the coating led to a change in morphology to an amorphous-crystalline structure. The crystallinity increased with increasing B concentration (Fig. 4b-d): nanometric structures with an average size of 200 nm were produced on top of clusters 1 and 2 μm in size (insets of Fig. 4b-d). Notably, unlike Ni-B coatings [7], in Co-B coatings, the size of surface microfissures decreased

until they disappeared with increasing B concentration (Co-B, 3 wt.% B), indicative of a low level of internal stress in the coatings. This result is associated with the low hydrogen concentration (below the detection limit of the GDS instrument) in the Co-B coating matrix, which was likely caused DMAB adsorbed onto the surface inhibiting the hydrogen evolution reaction.

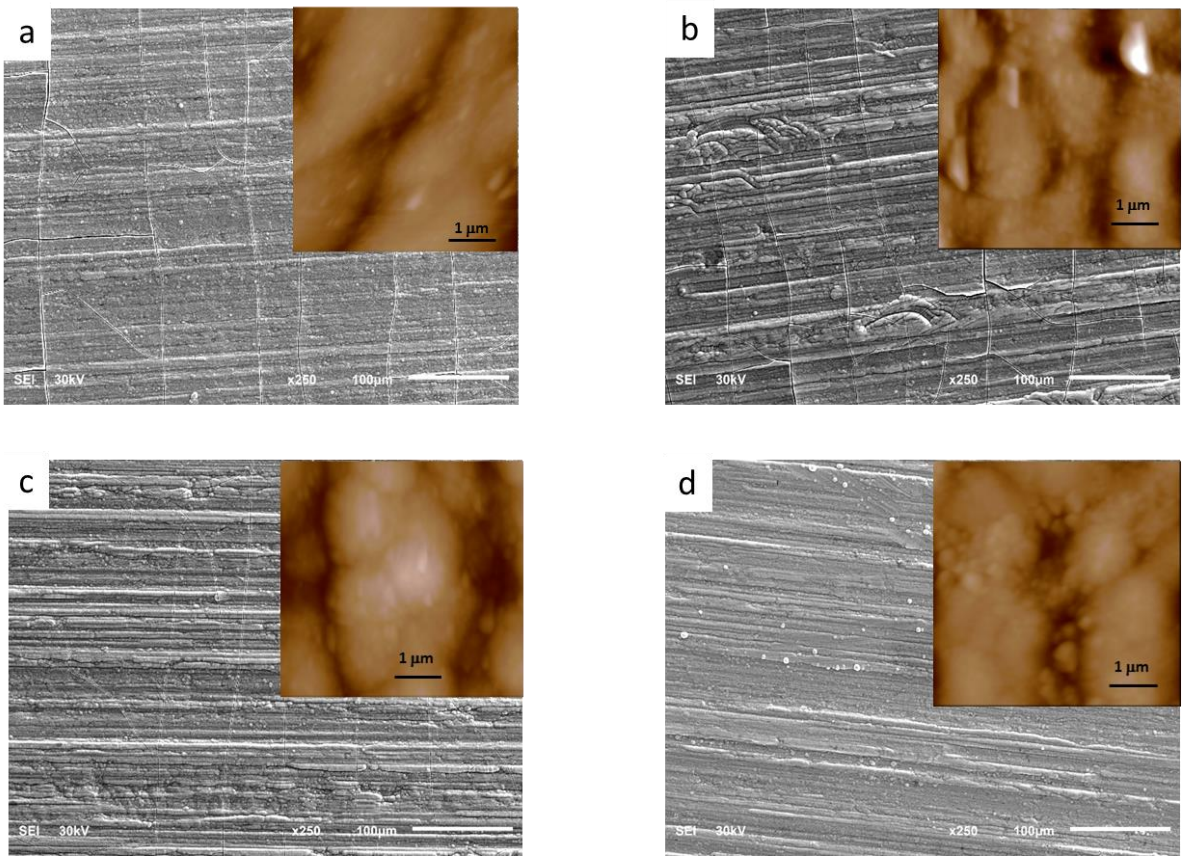

Figure 4. SEM and AFM images of the Co-B coatings with different boron contents obtained under galvanostatic conditions (j = 0.011 mA cm^{-2}, t = 45 min): a) 0 wt.% B, b) 1.5 wt.% B, c) 2.94 wt.% B and d) 3.0 wt.% B.

3.3 Tribological characterization

3.3.1 Microhardness of Co-B electrodeposits

Microhardness was measured for the Co-B coatings as a function of B concentration (Fig. 5). The results show that the hardness of the Co-B coatings increased with B concentration. When the concentration of B was less than or equal to 2.4 wt.% B, the hardness increased slightly; however, when the B concentration was increased from 2.4 to 2.9 wt.% B, the hardness increased substantially from 760.43 to 805.93 HV. This behaviour is associated with the incorporation of boron atoms within the cobalt crystalline matrix and to the distortion of interstitial positions causing a decrease in the mobility of dislocations [18]. This phenomenon favours strengthening of the electrochemical deposits.

The value of the maximum hardness, 818.17 HV, obtained for the Co-B coating (3 wt.% B) is higher than both that reported by Ogihara *et al.* (810 HV) [8] for Ni-B (4 at.% B) and that reported by Krishnaveni *et al.* (620 HV) [6] for Ni-B (3 wt.% B). It is somewhat lower than that for hard chromium coatings, which have been reported to exhibit a microhardness of 867.11 HV [37].

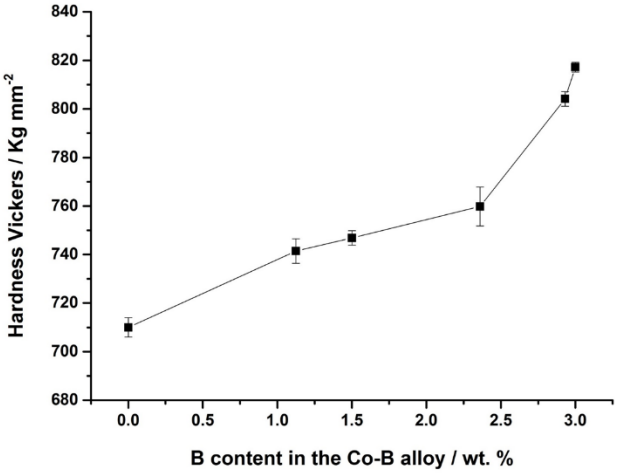

Figure 5. The relationship between boron content and hardness of the Co-B coatings obtained under galvanostatic conditions (j = 0.011 mA cm^{-2}, t = 20 min).

3.3.2 Wear resistance

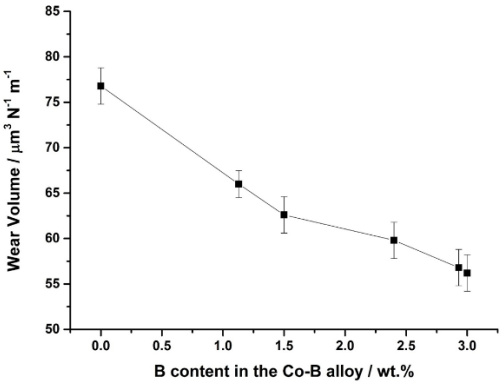

Figure 6. The relationship between boron content and wear volume of Co-B coatings obtained under galvanostatic conditions (j = 0.011 mA cm^{-2}, t = 20 min).

The results of the tribological tests show an improvement in the wear resistance of Co when it formed an alloy with boron. Fig. 6 shows the wear volume curves for the electrodeposited Co-B coatings with various amounts of B. As the concentration of B was increased in the Co-B coating, the wear volume decreased (*i.e.*, the wear resistance increased). No significant changes were observed in the wear volume at concentrations greater than 2.9 wt.% B. This behaviour is associated with the presence of microfissures in the surface of the Co-B coatings with a B content less than 2.9 wt.% (Fig.

4), which negatively influenced the abrasion resistance. Similarly, coatings with a concentration greater than or equal to 2.9 wt.% B showed higher crystallinity, presumably due to the formation of an interstitial-substitutional solid solution [38].

To understand the wear mechanism of the Co-B coatings with different B contents, we observed the wear track patterns using optical microscopy. As evident in Fig. 7, much adhesive tearing and many plough lines are observed along the sliding direction. Compared with the coating scars of other Co-B coatings, those for the coating with 3 wt.% B (Fig. 7c) exhibited the narrowest width and the shallowest depth of plough lines. These results indicate that the coating with 3 wt.% B exhibited the best wear resistance among the investigated coatings.

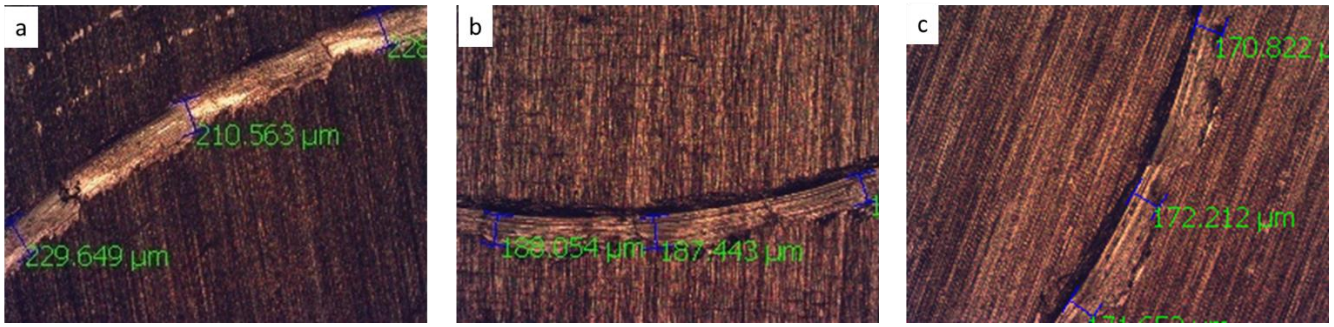

Figure 7. Optical micrograph of wear tracks after ball-on-disc wear tests for Co-B coatings: a) Co-B (0 wt.% B, b) Co-B (2.4 wt.% B), and c) Co-B (3 wt.% B).

The coefficients of friction were recorded simultaneously during the wear tests. The friction coefficient increased with increasing B content in the Co-B coatings (Fig. 8). The Co-B coating with 3 wt.% B exhibited a friction coefficient of 0.48, similar to the value reported by Lee *et al.* [39] for a Ni-B alloy and lower than that reported by Krishnaveni [6].

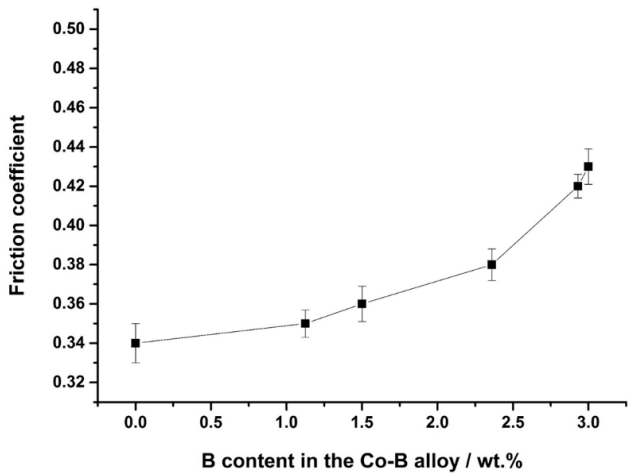

Figure 8. The relationship between the friction coefficient and boron content in the Co-B coatings.

4. CONCLUSIONS

In this study, we examined the influence of the DMAB concentration in the electrolytic bath on the elemental composition of Co-B coatings prepared via electrodeposition. Tribological characteristics such as hardness, wear volume and friction coefficient were evaluated as a function of the concentration of B in the coatings.

The GDS analysis of the chemical depth profile of the coatings showed an increase in the B concentration of the coatings from 1 to 3 wt.% when the concentration of DMAB in the electrolytic solution ranged from 1 to 10 g L^{-1}.

The XPS results indicate an electron transfer between B and Co in the Co-B coatings, likely due to formation of an interstitial/substitutional solid solution of B in the Co matrix. The formation of the solid solution may indicate the co-deposition of B in elemental form. The results of the GDS and XPS analysis of the Co-B coatings indicated the presence of DMAB in the coating, leading to the conclusion that DMAB was adsorbed onto the substrate surface during the electrodeposition process, where it was degraded during the co-deposition of B and Co.

The Co-B coatings prepared with different concentrations of B were adherent, smooth and shiny. Additionally, the microhardness of the coatings increased with increasing amount of B in the coatings. Co-B with 3 wt.% B showed no surface microfissures and therefore exhibited the best tribological properties: a microhardness of 818 HV, a wear volume of 56 $\mu m^3 N^{-1} m^{-1}$ and a coefficient of friction of 0.42. These values are higher than those reported for Ni-B coatings. Additional advantages include a lack of microfissures on the surface and the lack of a heat treatment. The hardness values were also slightly lower than those reported for hard Cr; therefore, the Co-B coating with 3 wt.% B may be viable alternatives to highly polluting coatings of hard Cr and Ni-B.

ACKNOWLEDGEMENTS

The authors gratefully acknowledge financial support from the Mexican Council for Science and Technology (CONACYT, projects CB-2013-0/221259 and PN/2015-01-248). Additionally, Alma Martínez acknowledges CONACYT for the graduate fellowships.

References

1. O.R. Monteiro, S. Murugesan, V. Khabashesku, *Surf. Coat. Tech*., 272 (2015) 291.
2. M. Onoda, K. Shimizu, Y. Tateishi, *Trans IMF*., 77 (1999) 44.
3. C.F. Malfatti, J. Zoppas Ferreira, C.B. Santos, B.V. Souza, E.P. Fallavena, S. Vaillant, J.P. Bonino, *Corros. Sci*., 47 (2005) 567.
4. Yu.N. Bekish, S.K. Poznyak, L.S. Tsybulskaya, T.V. Gaevskaya, *Electrochim. Acta*, 55 (2010) 2223.
5. Y.W. Riddle and T.O. Bailerare, *JOM*, 57 (2005) 40.
6. K. Krishnaveni, T.S.N. Sankara Narayanan, S.K. Seshadri, *Mater. Chem. Phys*., 99 (2006) 300.
7. J.R. López, P.F. Méndez, J.J. Pérez-Bueno, G. Trejo, G. Stremsdoerfer, Y, Meas, *Int. J. Electrochem. Sci*., 11 (2016) 4231.
8. H. Ogihara, K. Udagawa, T. Saji, *Surf. Coat. Technol*., 206 (2012) 2933.
9. Y.S. Huang and F.Z Cui, *Surf. Coat. Tech*., 201 (2007) 5416.
10. S. Alirezaei, S.M. Monirvaghefi, M. Salehi, A. Saatchi, *Wear*, 262 (2007) 978.

11. D. Nava, C.E. Dávalos, A. Martínez-Hernández, F. Manríquez, Y. Meas, R. Ortega-Borges, J.J. Pérez-Bueno, G. Trejo, *Int. J. Electrochem. Sci.*, 8 (2013) 2670.
12. L. Wang, Y. Gao, T. Xu, Q. Xue, *Appl. Surf. Sci*., 252 (2006) 7361.
13. Z. Shi, D. Wang, Z. Ding, *Appl. Surf. Sci*., 221 (2004) 62.
14. B. Oraon, C. Majumdar, B. Ghosh, *Mater. Des*., 29 (2008) 1412.
15. H. Ogihara, H. Wang, T. Saji, *Appl. Surf. Sci*., 296 (2014) 108.
16. T.S.N. Sankara Narayanan, K. Krishnaveni, S.K. Seshadri, *Mater. Chem. Phys*., 82 (2003) 771.
17. M.I.S.T. Faria, T. Leonardi, G.C. Cowlho, C.A. Nunes, R.R. Avillez, *Mater. Charact*., 58 (2007) 358.
18. C. Lerner and M.C. Cadeville, *Scripta Metall. Mater*., 7 (1973) 941.
19. J.O. Duruibe, M.O.C. Ogwuegbu, J.N. Egwurugwu, *Int. J. Phys. Sci*., 2 (2007) 112.
20. H. Li, Y. Wu, H. Luo, M. Wang, Y. Xu, *J. Catal*., 214 (2003) 15.
21. L. Hui, W. Chengzuo, Qingfei Z., L. Hexing, *Appl. Surf. Sci*., 254 (2008) 7516.
22. D.S. Lu, W.S. Li, X. Jiang, C.L. Tan, R.H. Zeng, *J. Alloys Compd*., 485 (2009) 621.
23. L. Yi, W. Yijing, X. Lingling, S. Dawei, W. Yaping, J. Lifang, Y. Huatang, *Electrochim. Acta*, 53 (2008) 2265.
24. Y.D. Wang, X.P. Ai, H.X. Yang, *Chem. Mater.*, 16 (2004) 5194.
25. Y. Wang, L. Li, W.Y. Wang, D. Song, G. Liu, Y. Han, L. Jiao, H. Yuan, *J. Power Sources*, 196 (2011) 5731.
26. D.S. Lu, W.S. Li, X. Jiang, C.L. Tan, Q.M. Huang, *Electrochim. Acta* 56 (2011) 4540.
27. M. Anik, N. Kücükdeveci, A. Yilmaz, *Thin solid films* 527 (2013) 69.
28. P. Gao, S. Yang, Z. Xue, G. Liu, G. Zhang, L. Wang, G. Li, Y. Sun, Y Chen, *J. Alloy Compd*. 239 (2012) 90.
29. N. Patel and A. Miotello, *Int. J. Hydrogen Energ.*, 40 (2015) 1429.
30. A. Subramanian, C. Shunmuganathan, T. Vasudevan, V.S. Muralidharan, *Trans IMF* 79 (2001) 119.
31. Y.N. Bekish, S.S. Grabchikov, L.S. Tsybul´skaya, V.A. Kukareko, S.S. Perevoznikov, *Prot. Met. and Phys. Chem. Surf*., 49 (2013) 319.
32. 2004 Annual Book of ASTM Standards, Wear and Erosion; Metal Corrosion. P.C. Fazio et al. Editors, ASTM G102-89. Standard Practice for Calculation of Corrosion rates and related Information from Electrochemical Measurements, ASTM, Philadelphia, (2004).
33. A. Brenner, Electrodeposition of alloys: principles and practice, vol. 1, P. 78., Academic Press, (1963) N.Y. USA,
34. C.D. Wagner, W.M. Riggs, L.E. Davis, Hand-book of X-ray Photoelectron Spectroscopy, (1979) Nerwalk: Perkin Elmer p 55344.
35. N.S. McIntyre, D.D. Johnston, L.L. Coatsworth, *Surf. Interface Anal*., 15 (1990) 265.
36. Li Hui, Li Hexing, Deng Jing-Fa, *Mater. Lett.*, 50 (2001) 41.
37. S. Villant, L. Datas, J.P. Bonino, *Matériaux and Techniques*, 11-12 (2001) 47.
38. L.S. Tsybul´skaya, V.A. Kukareko, Yu.N. Bekish, T.V. Gaevskaya, A.G. Kononov, *Russ. J. Appl. Chem*., 81 (2008) 1554.
39. K.H. Lee, D. Chang, S.C. Kwon, *Electrochim. Acta*, 50 (2005) 4538.